

Structure and excitations of liquid-helium films

Janice L. Epstein and Eckhard Krotschek

Center for Theoretical Physics, Department of Physics, Texas A&M University, College Station, Texas 77843-4242

(Received 15 May 1987)

We study the structure and the spectrum of elementary excitations of films of ^4He atoms adsorbed to plane substrates of varying strengths. An optimized variational description of the ground-state wave function provides the short- and long-ranged structure, the distribution functions, the dispersion relations, and the spatial shape of the collective modes.

I. INTRODUCTION

The study of helium films adsorbed to substrates in the low-temperature regime is presently an area of active experimental research.¹ Among the variety of experiments, electron-mobility² and third-sound^{3,4} measurements directly probe the discrete layer structure of the adsorbed liquid. Closely related questions are the study of collective excitations⁵ and the problem of the stability of adsorbed liquids against longitudinal density fluctuations, manifested in solidification of the liquid close to the substrate^{6,7} and the "wetting" behavior of the liquid.^{8,9}

For a microscopic theoretical interpretation of these effects, a theory is necessary that reveals the layer structure of the films and provides a consistent description of the ground-state and the collective excitations. Such a microscopic theory has been developed recently¹⁰ starting from a variational ansatz for the ground-state wave function of the Feenberg form,¹¹

$$\Psi_0(\mathbf{r}_1, \dots, \mathbf{r}_A) = \exp \left[\frac{1}{2} \sum_{1 \leq i \leq A} u_1(\mathbf{r}_i) + \frac{1}{2} \sum_{1 \leq i < j \leq A} u_2(\mathbf{r}_i, \mathbf{r}_j) + \dots \right]. \quad (1.1)$$

The $u_n(\mathbf{r}_1, \mathbf{r}_2, \dots, \mathbf{r}_n)$ are n -body correlation factors; they vanish whenever one or more of the particles is moved far away from the rest. The ansatz (1.1) is especially suitable for Bose systems, where it is in principle an exact representation of the ground-state wave function.

The wave function (1.1) for the so-called "Jastrow choice" $u_n(\mathbf{r}_1, \dots, \mathbf{r}_n) = 0$ for $n > 2$ has been used successfully to describe inhomogeneous quantum systems. A central part of the theory is the optimization of the microscopic wave function by minimizing the energy expectation value

$$H_{00} = \frac{(\Psi_0 | H | \Psi_0)}{(\Psi_0 | \Psi_0)}, \quad (1.2)$$

$$\frac{\delta H_{00}}{\delta u_1}(\mathbf{r}) = 0, \quad \frac{\delta H_{00}}{\delta u_2}(\mathbf{r}, \mathbf{r}') = 0. \quad (1.3)$$

The simplest acceptable approximation of the energy-expectation value that allows a meaningful optimization

of the correlations is the hypernetted-chain (HNC) approximation which we shall use throughout this paper. The approximation has well-known deficiencies^{12,13} for dense systems like ^4He . But it is the simplest theory that provides the qualitative physical features, starting from no other information than the microscopic Hamiltonian. No simplifying assumption on the form of the two-body correlations (as, for example, isotropy) needs to be made. An especially desirable feature of the theory is that it provides the form and the dispersion relation of the collective excitations as a natural by-product of the optimization of the ground state.

The variational theory of the ground state and its extension to excited states has been reviewed in Ref. 10. In the next section we will display only the basic definitions and equations. Section III presents the results of extensive calculations of the structure of helium films on substrates of three different strengths. Depending on the substrate potential, we find up to five clearly defined layers of helium atoms. Section IV discusses the dispersion relations of the collective modes and the surface-structure function and compares the excitation spectra for different substrates and different surface coverages.

Special attention will be paid to the long-wavelength limit of the collective excitations in Sec. V. We obtain an explicit expression for the third-sound velocity in terms of microscopically defined quantities, and compare our results with the experimental data of Maynard and Chan.³

Section VI gives a brief summary of our results and the anticipated further developments.

II. VARIATIONAL THEORY

We consider a system of interacting particles in an external one-body potential; i.e., the Hamiltonian of the system is of the form

$$H = -\frac{\hbar^2}{2m} \sum_{i=1}^A \nabla_i^2 + \sum_{i=1}^A U_{\text{sub}}(\mathbf{r}_i) + \sum_{1 \leq i < j \leq A} v(|\mathbf{r}_i - \mathbf{r}_j|). \quad (2.1)$$

To be specific, we will assume that the external field depends on only one coordinate, say z . In this geometry, the one-body factor $u_1(\mathbf{r})$ and the one-body density

$$\rho_1(\mathbf{r}_1) = A \frac{\int d^3r_2 \int \cdots \int d^3r_A \Psi_0^2(\mathbf{r}_1, \dots, \mathbf{r}_A)}{\int d^3r_1 \int \cdots \int d^3r_A \Psi_0^2(\mathbf{r}_1, \dots, \mathbf{r}_A)} \quad (2.2)$$

depend only on z ; the two-body correlations $u_2(\mathbf{r}_1, \mathbf{r}_2)$, the two-body density

$$\begin{aligned} \rho_2(\mathbf{r}_1, \mathbf{r}_2) \\ = A(A-1) \frac{\int d^3r_3 \int \cdots \int d^3r_A \Psi_0^2(\mathbf{r}_1, \dots, \mathbf{r}_A)}{\int d^3r_1 \int \cdots \int d^3r_A \Psi_0^2(\mathbf{r}_1, \dots, \mathbf{r}_A)}, \end{aligned} \quad (2.3)$$

and the two-body distribution function

$$g(\mathbf{r}_1, \mathbf{r}_2) = \frac{\rho_2(\mathbf{r}_1, \mathbf{r}_2)}{\rho_1(\mathbf{r}_1)\rho_1(\mathbf{r}_2)} \quad (2.4)$$

$$v_{\text{JF}}(\mathbf{r}_1, \mathbf{r}_2) = v(|\mathbf{r}_1 - \mathbf{r}_2|) - \frac{\hbar^2}{8m} \left[\frac{1}{\rho_1(\mathbf{r}_1)} \nabla_{\mathbf{r}_1} \rho_1(\mathbf{r}_1) \cdot \nabla_{\mathbf{r}_1} + \frac{1}{\rho_1(\mathbf{r}_2)} \nabla_{\mathbf{r}_2} \rho_1(\mathbf{r}_2) \cdot \nabla_{\mathbf{r}_2} \right] u_2(\mathbf{r}_1, \mathbf{r}_2). \quad (2.8)$$

The relation between the two-body density and the two-body correlation factor is provided by the hypernetted-chain equations,

$$\begin{aligned} g(\mathbf{r}_1, \mathbf{r}_2) &= \frac{\rho_2(\mathbf{r}_1, \mathbf{r}_2)}{\rho_1(\mathbf{r}_1)\rho_1(\mathbf{r}_2)} \\ &= \exp[u_2(\mathbf{r}_1, \mathbf{r}_2) + N(\mathbf{r}_1, \mathbf{r}_2) + E(\mathbf{r}_1, \mathbf{r}_2)] - 1, \end{aligned} \quad (2.9a)$$

$$X(\mathbf{r}_1, \mathbf{r}_2) = g(\mathbf{r}_1, \mathbf{r}_2) - 1 - N(\mathbf{r}_1, \mathbf{r}_2), \quad (2.9b)$$

$$N(\mathbf{r}_1, \mathbf{r}_2) = \int d^3r_3 \rho_1(\mathbf{r}_3) [g(\mathbf{r}_1, \mathbf{r}_3) - 1] X(\mathbf{r}_3, \mathbf{r}_2). \quad (2.9c)$$

The level of sophistication of the theory is defined by the choice of the approximation for the "elementary diagram sum" $E(\mathbf{r}_1, \mathbf{r}_2)$. The simplest choice is the "HNC approximation," $E(\mathbf{r}_1, \mathbf{r}_2) = 0$; this is also the simplest possible approximation that allows a meaningful optimization of the ground state; we shall use it throughout our paper. The approximation introduces numerical uncertainties of a size similar to those caused by the omission of three-body correlations.^{12,13}

For a compact representation of the Euler-Lagrange (EL) equations (1.3) it is useful to introduce some nota-

tion. For any two-point function $A(\mathbf{r}_1, \mathbf{r}_2)$ we abbreviate

$$H_{00} = (\Delta E_1) + (\Delta E_2), \quad (2.5)$$

with

$$(\Delta E_1) = \int d^3r \rho_1(\mathbf{r}) \left[U_{\text{sub}}(\mathbf{r}) + \frac{\hbar^2}{2m} |\nabla \sqrt{\rho_1(\mathbf{r})}|^2 \right] \quad (2.6)$$

and

$$(\Delta E_2) = \frac{1}{2} \int d^3r_1 d^3r_2 \rho_2(\mathbf{r}_1, \mathbf{r}_2) v_{\text{JF}}(\mathbf{r}_1, \mathbf{r}_2). \quad (2.7)$$

$v_{\text{JF}}(\mathbf{r}_1, \mathbf{r}_2)$ is the generalized Jackson-Feenberg interaction

tion. For any two-point function $A(\mathbf{r}_1, \mathbf{r}_2)$ we abbreviate

$$\tilde{A}(\mathbf{r}_1, \mathbf{r}_2) \equiv \sqrt{\rho_1(\mathbf{r}_1)} A(\mathbf{r}_1, \mathbf{r}_2) \sqrt{\rho_1(\mathbf{r}_2)}. \quad (2.10)$$

The convolution product of two functions $A(\mathbf{r}_1, \mathbf{r}_2)$ and $B(\mathbf{r}_1, \mathbf{r}_2)$ is written as

$$[\tilde{A} * \tilde{B}](\mathbf{r}_1, \mathbf{r}_2) = \int d^3r_3 \tilde{A}(\mathbf{r}_1, \mathbf{r}_3) \tilde{B}(\mathbf{r}_3, \mathbf{r}_2) \quad (2.11)$$

and

$$H_1 \equiv -\frac{\hbar^2}{2m} \frac{1}{\sqrt{\rho_1(\mathbf{r})}} \nabla \rho_1(\mathbf{r}) \cdot \nabla \frac{1}{\sqrt{\rho_1(\mathbf{r})}}. \quad (2.12)$$

The Euler-Lagrange equation for the two-body correlations is most conveniently written in a random-phase approximation (RPA) form in which the sets of "non-nodal diagrams" $X(\mathbf{r}_1, \mathbf{r}_2)$ [cf. Eq. (2.9b)] are related to the particle-hole interaction $V_{p-h}(\mathbf{r}_1, \mathbf{r}_2)$. This form is best suited for an economical numerical treatment and the study of excited states. The equations are

$$-[H_1 * \tilde{X} + \tilde{X} * H_1 - \tilde{X} * H_1 * \tilde{X}](\mathbf{r}_1, \mathbf{r}_2) = 2\tilde{V}_{p-h}(\mathbf{r}_1, \mathbf{r}_2), \quad (2.13)$$

with

$$V_{p-h}(\mathbf{r}_1, \mathbf{r}_2) = g(\mathbf{r}_1, \mathbf{r}_2) v(|\mathbf{r}_1 - \mathbf{r}_2|) + \frac{\hbar^2}{2m} [|\nabla_1 \sqrt{g(\mathbf{r}_1, \mathbf{r}_2)}|^2 + |\nabla_2 \sqrt{g(\mathbf{r}_1, \mathbf{r}_2)}|^2] + [g(\mathbf{r}_1, \mathbf{r}_2) - 1] w_I(\mathbf{r}_1, \mathbf{r}_2), \quad (2.14)$$

$$\tilde{w}_I(\mathbf{r}_1, \mathbf{r}_2) = -\frac{1}{2} [H_1 * \tilde{N} + \tilde{N} * H_1 + \tilde{X} * H_1 * \tilde{X}](\mathbf{r}_1, \mathbf{r}_2). \quad (2.15)$$

The one-body density is obtained by minimizing the energy under the constraint of constant particle number A . The corresponding Euler equation has the form of a Hartree equation for the square root of the one-body density,

$$-\frac{\hbar^2}{2m}\nabla^2\sqrt{\rho_1(\mathbf{r})}+[U_{\text{sub}}(\mathbf{r})+V_H(\mathbf{r})]\sqrt{\rho_1(\mathbf{r})}=\mu\sqrt{\rho_1(\mathbf{r})}, \quad (2.16)$$

where μ is the chemical potential, and $V_H(\mathbf{r})$ a generalized Hartree potential

$$V_H(\mathbf{r})=\frac{\delta(\Delta E_2)}{\delta\rho_1(\mathbf{r})}. \quad (2.17)$$

The Hartree potential $V_H(\mathbf{r})$ can again be expressed in terms of the compound-diagrammatic constituents of the HNC theory. Its explicit form has been given in Ref. 10,

$$V_H(\mathbf{r}_1)=V_H^{(1)}(\mathbf{r}_1)+V_H^{(2)}(\mathbf{r}_1), \quad (2.18)$$

with

$$V_H^{(1)}(\mathbf{r}_1)=\int d^3r_2\rho_1(\mathbf{r}_2)\{V_{p-h}(\mathbf{r}_1,\mathbf{r}_2)-\frac{1}{2}[g(\mathbf{r}_1,\mathbf{r}_2)-1]\omega_I(\mathbf{r}_1,\mathbf{r}_2)\} \quad (2.19)$$

and

$$V_H^{(2)}(\mathbf{r}_2)=-\frac{\hbar^2}{16m\rho_1(\mathbf{r}_1)}\nabla\rho_1(\mathbf{r}_1)\cdot\nabla\int d^3r_2\rho_1(\mathbf{r}_2)[g(\mathbf{r}_1,\mathbf{r}_2)-1]N(\mathbf{r}_1,\mathbf{r}_2). \quad (2.20)$$

The numerical solution of the two-body Euler equation (2.13) is intimately connected to the theory of collective excitations.¹⁰ The energies of the collective modes are derived from the eigenvalue problem

$$[H_1+2\tilde{V}_{p-h}]^*H_1\psi^{(l)}=\hbar^2\omega_l^2\psi^{(l)}. \quad (2.21)$$

The eigenstates of $\psi^{(l)}$ of (2.21) are normalized such that

$$(\psi^{(l)}|H_1|\psi^{(l')})=\delta_{l,l'}. \quad (2.22)$$

From these states we can construct the response function

$$\chi(\mathbf{r},\mathbf{r}',\omega)=2[\rho_1(\mathbf{r})]^{1/2}\sum_l\left\{\frac{[H_1\psi^{(l)}](\mathbf{r})}{\hbar^2\omega^2-\hbar^2\omega_l^2}[H_1\psi^{(l)}](\mathbf{r}')\right\}[\rho_1(\mathbf{r}')]^{1/2} \quad (2.23)$$

and its inverse

$$\chi^{-1}(\mathbf{r},\mathbf{r}',\omega)=\frac{1}{2}\sum_l\frac{\psi^{(l)}(\mathbf{r})}{[\rho_1(\mathbf{r})]^{1/2}}(\hbar^2\omega^2-\hbar^2\omega_l^2)\frac{\psi^{(l)}(\mathbf{r}')}{[\rho_1(\mathbf{r}')]^{1/2}}. \quad (2.24)$$

From the orthogonality relation (2.22) we see immediately that the normal modes of the system are given by

$$\delta\rho_{(l)}^{1/2}(\mathbf{r},\omega)\equiv\frac{\delta\rho_{(l)}(\mathbf{r},\omega)}{2\sqrt{\rho_1(\mathbf{r})}}\sim[H_1\psi^{(l)}](\mathbf{r})\delta(\omega-\omega_l). \quad (2.25)$$

The static form factor is calculated from the response function (2.23) by frequency integration,

$$S(\mathbf{r}_1,\mathbf{r}_2)=\frac{1}{\sqrt{\rho_1(\mathbf{r}_1)\rho_1(\mathbf{r}_2)}}\int\frac{d(\hbar\omega)}{2\pi}\text{Im}\chi(\mathbf{r}_1,\mathbf{r}_2,\omega) \\ =\sum_l\frac{1}{\hbar\omega_l}[H_1\psi^{(l)}(\mathbf{r}_1)][H_1\psi^{(l)}(\mathbf{r}_2)]. \quad (2.26)$$

We may now also obtain the two-body distribution function

$$g(\mathbf{r}_1,\mathbf{r}_2)=1+\frac{S(\mathbf{r}_1,\mathbf{r}_2)-\delta(\mathbf{r}_1-\mathbf{r}_2)}{\sqrt{\rho_1(\mathbf{r}_1)}\sqrt{\rho_1(\mathbf{r}_2)}} \quad (2.27)$$

and the set $X(\mathbf{r}_1,\mathbf{r}_2)$ of non-nodal diagrams.

$$\delta(\mathbf{r}_1-\mathbf{r}_2)-\sqrt{\rho_1(\mathbf{r}_1)}X(\mathbf{r}_1,\mathbf{r}_2)\sqrt{\rho_1(\mathbf{r}_2)} \\ =\sum_l\hbar\omega_l\psi^{(l)}(\mathbf{r}_1)\psi^{(l)}(\mathbf{r}_2). \quad (2.28)$$

Equations (2.26)–(2.28) are used for the numerical solution of the Euler-Lagrange equation.

III. GROUND-STATE STRUCTURE

The physical model underlying our calculations is a number of helium atoms interacting via the Aziz potential.¹⁴ The atoms are adsorbed to a substrate which is described by an external field $U_{\text{sub}}(z)$. A simple form for $U_{\text{sub}}(z)$ is the potential obtained by averaging Lennard-Jones interactions between helium and substrate atoms over a half-space.^{15,16} One obtains

$$U_{\text{sub}}(z)=e\left[\frac{1}{15}\left(\frac{s}{z}\right)^9-\left(\frac{s}{z}\right)^3\right]. \quad (3.1)$$

Given the substrate potential, the two-body interaction, and the surface coverage

$$n=\int dz\rho_1(z), \quad (3.2)$$

the physical model is completely defined. It is an oversimplification in the sense that the real substrate potentials are not translationally invariant in the x - y plane due to the crystal structure of the substrate. Moreover,

the interaction between the two individual helium atoms is changed in the presence of a substrate^{16,17} due to the substrate screening of the van der Waals interaction and induced three-body forces.¹⁸ These effects are ignored in the present work.

A second point that has been disregarded in our work is that the first one or two layers of an adsorbed helium film are expected to be solid.^{6,7} The instability against a liquid-solid phase transition appears in the HNC theory in the form of an instability of the HNC-EL equations for the *liquid* phase against density fluctuations of finite wavelength.¹⁹ This feature of a theory is, in principle, quite desirable, but the simultaneous description of a liquid and a solid phase is presently beyond our computational capabilities. Before one gets close to the *local* instability against finite-wavelength density fluctuations, the pair-distribution functions $g(r_1, r_2)$ develop strong, long-ranged oscillations, and the numerical treatment becomes quite cumbersome. In order to avoid such an instability of the theory in the very dense regime close to the substrate, it was necessary to weaken the most attractive part of the substrate potential.

We have extended the calculations of Ref. 10 to an additional medium-strength substrate potential and have solved Eqs. (2.13)–(2.20) for a large number of surface coverages n . Two of our substrate potentials are of the form (3.1). They are characterized by the strength e and the range s appearing in Eq. (3.1). The strongest potential (called model I) is a substrate potential of the form (3.1) fitted to the strength of the attractive tail of the helium-graphite interaction. The potential parameters are $e = 48$ K and $s = 3.6$ Å, which is about midway between the theoretical and experimental predictions quoted in Ref. 16. The attractive tail of the potential has a

strength (the Hamaker constant) of $A_\infty = 2240$ K Å³. The second potential, model II, uses the attractive part of the Carlos-Cole potential,¹⁷ i.e., $e = 34$ K, and $s = 3.6$ Å, which leads to $A_\infty = 1586$ K Å³. For the reasons discussed above, the repulsive part has been enhanced. Thus, the potential depth of model I is just 72 K, whereas the second potential has a depth of 51 K.

Our third substrate potential²⁰ describes a system where a thin film of solid H₂ of about 10-Å thickness is adsorbed to a glass surface. The potential form is

$$U_{\text{sub}}(z) = -\frac{435}{z^3} - \frac{1.5 \times 10^4}{z^5} + \frac{0.9 \times 10^6}{z^9} - \frac{915}{(z+10)^3}. \quad (3.3)$$

[$U_{\text{sub}}(z)$ is given in K, and z in Å]. The last term is due to the attraction of the underlying glass surface. The potential is the weakest of the three potentials used here. No enhancement of the repulsive part has been necessary in this case.

Figures 1–3 show the one-body densities $\rho_1(z)$ for the three potential models for helium films of different surface coverages n . The coordinate system has been chosen such that the zero point of the substrate potential is at $z_0 = 1.8$ Å. One sees clearly the formation of additional layers as the surface coverage is increased. The two stronger potential models show the formation of at least five layers, and it is not clear whether the formation of one or even two additional layers should be expected. Our present computational capabilities did not allow us to go to larger surface coverages. We feel also that the results of such extensions would be, due to the limitations of the HNC approximation, not sufficiently con-

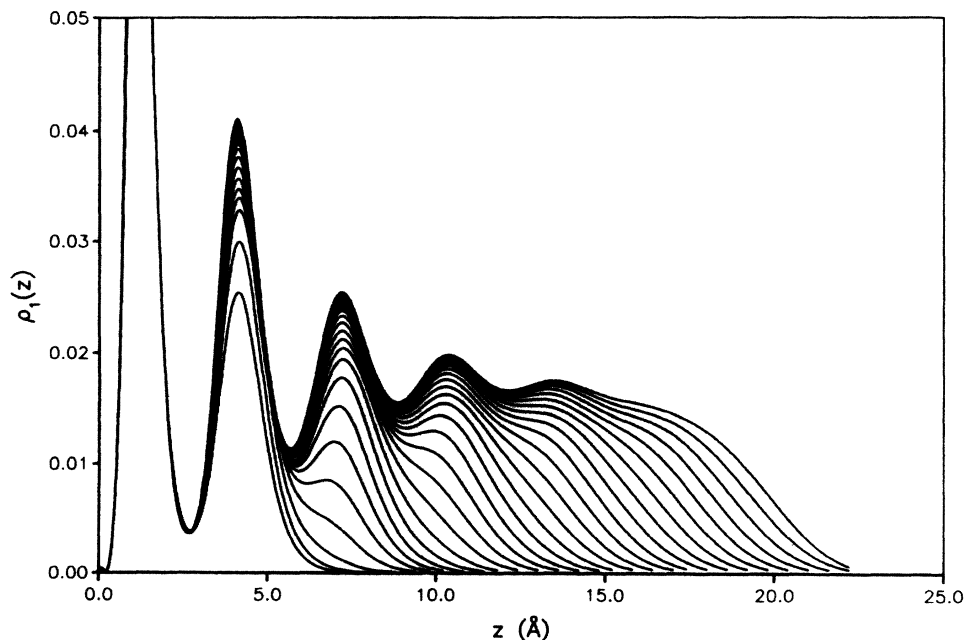


FIG. 1. The density profiles for helium films are shown for the strong substrate potential, model I, for particle numbers $n = 0.12$ – 0.39 Å⁻² in steps of 0.01 Å⁻². The substrate is located at negative z .

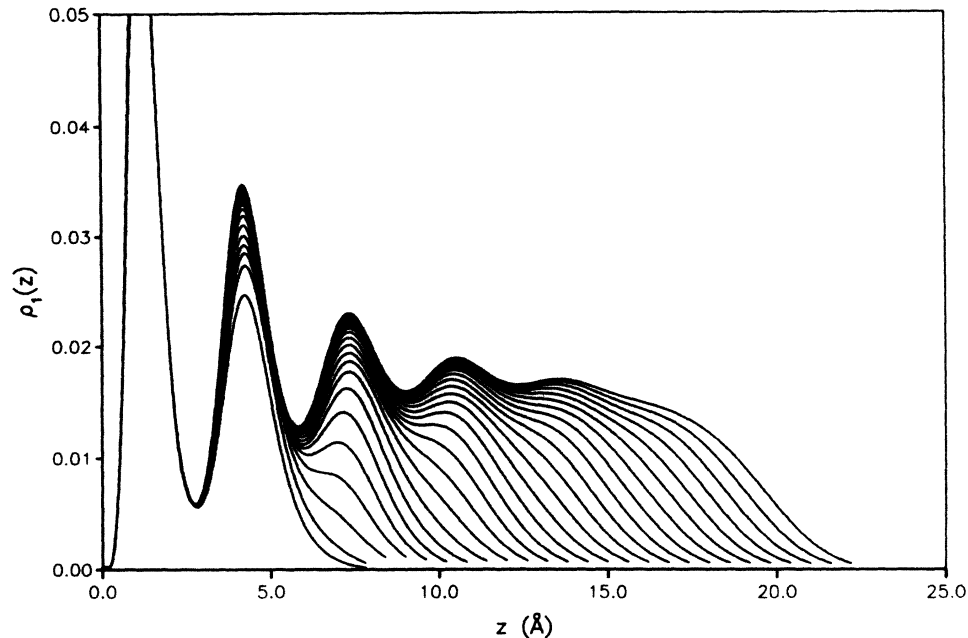


FIG. 2. Same as Fig. 1 for the medium-strength substrate potential model. The particle numbers are $n = 0.12-0.37 \text{ \AA}^{-2}$ in steps of 0.01 \AA^{-2} .

clusive to warrant the effort. The glass-hydrogen potential (Fig. 3) serves to illustrate the transition to the asymptotic region. Only four clearly distinguishable layers are formed; with increasing surface coverage we find a broad shoulder in the density profile.

We have attempted to increase the strength of the substrate potential in small steps in order to perform calculations for a potential that is closer to the Carlos-Cole potential. Keeping the attractive part, A_∞ , fixed, we were able to increase the short-ranged attraction to

about -100 K , which still falls short of the value of -220 K suggested by the Carlos-Cole potential. With increasing density, the pair-distribution function develops strong, long-ranged oscillations,¹⁹ and the calculations need to be carried out in a much larger box.

Our results for the ground-state energies and the chemical potentials for the three models under consideration are collected in Figs. 4 and 5. The energy per particle (Fig. 4) is seen to be still far from its asymptotic value of -5.4 K in the HNC approximation. The

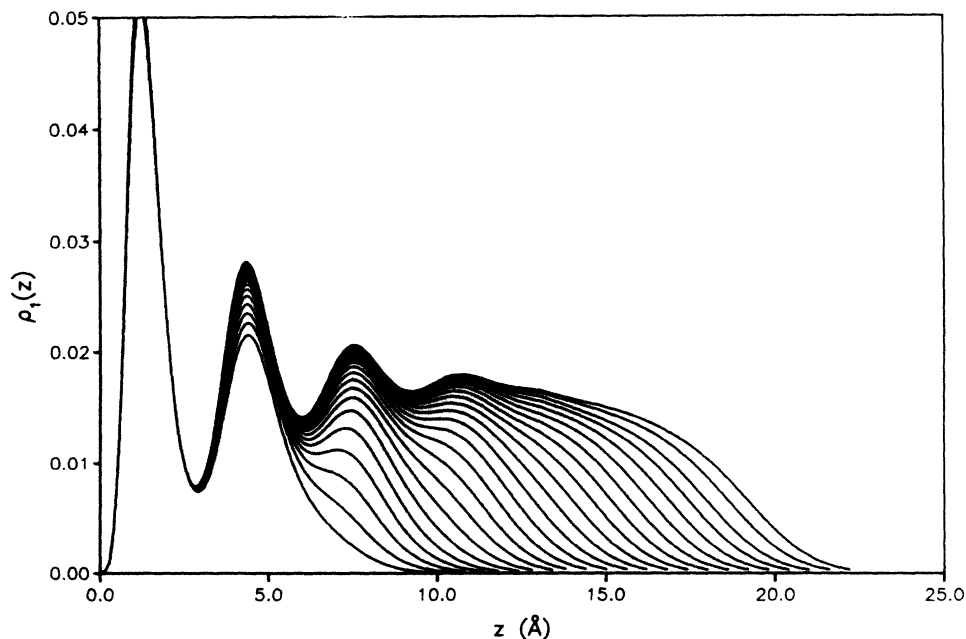


FIG. 3. Same as Fig. 1 for the hydrogen substrate potential. The particle numbers are $n = 0.12-0.34 \text{ \AA}^{-2}$ in steps of 0.01 \AA^{-2} .

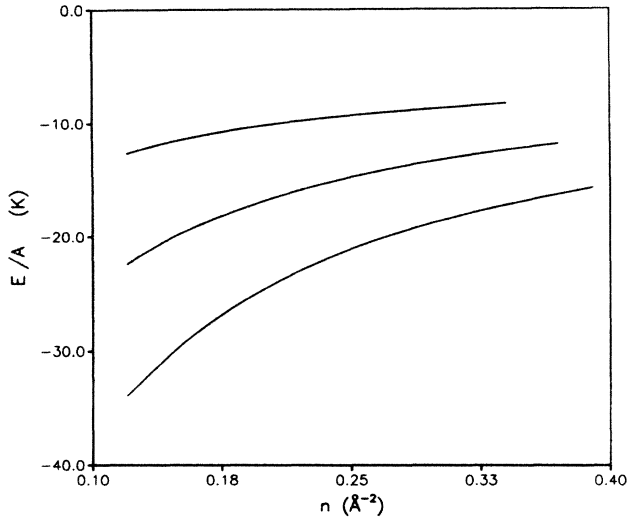


FIG. 4. The energy per particle is shown for the three different substrate potentials, as a function of the surface coverage n . The highest curve corresponds to the glass-hydrogen substrate, and the lowest curve to the strongest potential.

chemical potential μ approaches this value reasonably fast (Fig. 5); we interpret the difference of about 0.2 K as being due to the sacrifices made in our numerical treatment in order to keep the computational effort to a minimum. It should also be kept in mind that the chemical potential is the least stable quantity in our calculation; it is therefore affected by the largest numerical uncertainty. One of the causes of this numerical uncertainty is that one cannot extend the calculations too far into the very low-density tail of the film. The restriction of the calculation to a box that is as small as possible has the additional effect of rising the chemical potential slightly. We presently do not consider this a major drawback to the other parts of our calculations.

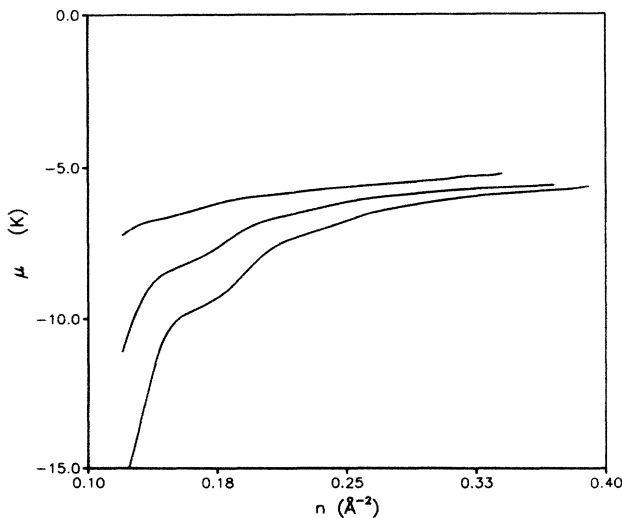


FIG. 5. The chemical potential is shown for the three different substrate potentials. The highest curve corresponds to the glass-hydrogen substrate, and the lowest curve to the strongest potential.

Whereas the energy per particle is a smooth function of the surface coverage n , the chemical potential shows a structure that is obviously related to the layering of the films. Despite the reservations pointed out above on the numerical accuracy of the calculation of the chemical potential, we consider these fluctuations numerically significant. Our results on the static properties of the helium films are entirely consistent with those found in Ref. 10. Small deviations for the potentials I and III are due to an improved numerical treatment. The much more extensive calculations were necessary to study the transition between the layer structure of the film and the asymptotic region in model III, and to permit the study of the third-sound velocity as a function of the layer thickness.

For the strongest substrate potential, Figs. 6 and 7 show the pair-correlation function $g(z, z, r_{\parallel})$ parallel to the surface as a function of the distance z from the substrate. In Fig. 6, we show $g(z, z, r_{\parallel})$ at the points of the five density maxima of the film with a surface coverage of $n = 0.37 \text{ \AA}^{-2}$. One can see clearly how the nearest-neighbor peak becomes weaker and moves further away from the coordinate origin as one goes to the lower-density regime. Similarly, the highest-density distribution function shows the strong oscillations mentioned above, which are typical for a high-density system.

Figure 7 shows the pair-distribution function, for the same example, at the locations of the *density minima* of the film. Corresponding to the very low density between the first two layers, the nearest-neighbor peak of the pair-distribution function in that regime is rather small and *increases* as one goes further out in the film. However, the wavelength of the oscillations is very close to the one of the pair-distribution function for the neighboring density maxima. Only the pair-distribution function in the surface region (at approximately half the saturation density) shows no oscillations at all. In this area, the distribution function is indeed similar to the one of a low-density bulk liquid.

IV. COLLECTIVE EXCITATIONS AND STATIC STRUCTURE FUNCTION

The spectrum of collective excitations can be measured, for example, by neutron scattering experiments.^{5,21} With improved intensity, the measurement of the static structure function $S(\mathbf{r}, \mathbf{r}')$ is expected to be feasible in the near future.²² The low-energy-long-wavelength part of the excitation spectrum is finally observable by third-sound^{3,4} and electron-mobility measurements² which clearly exhibit the dependence of the low-energy excitations spectrum of the layer structure and the thickness of the film.

Hydrodynamic theories predict a dispersion relation of the form

$$\omega^2(q_{\parallel}) = \left[g' q_{\parallel} + \frac{\sigma}{m\rho} q_{\parallel}^3 \right] \tanh(q_{\parallel} d), \quad (4.1)$$

where ρ , σ , and g' are the density, surface tension, and van der Waals acceleration of the liquid. d is the film

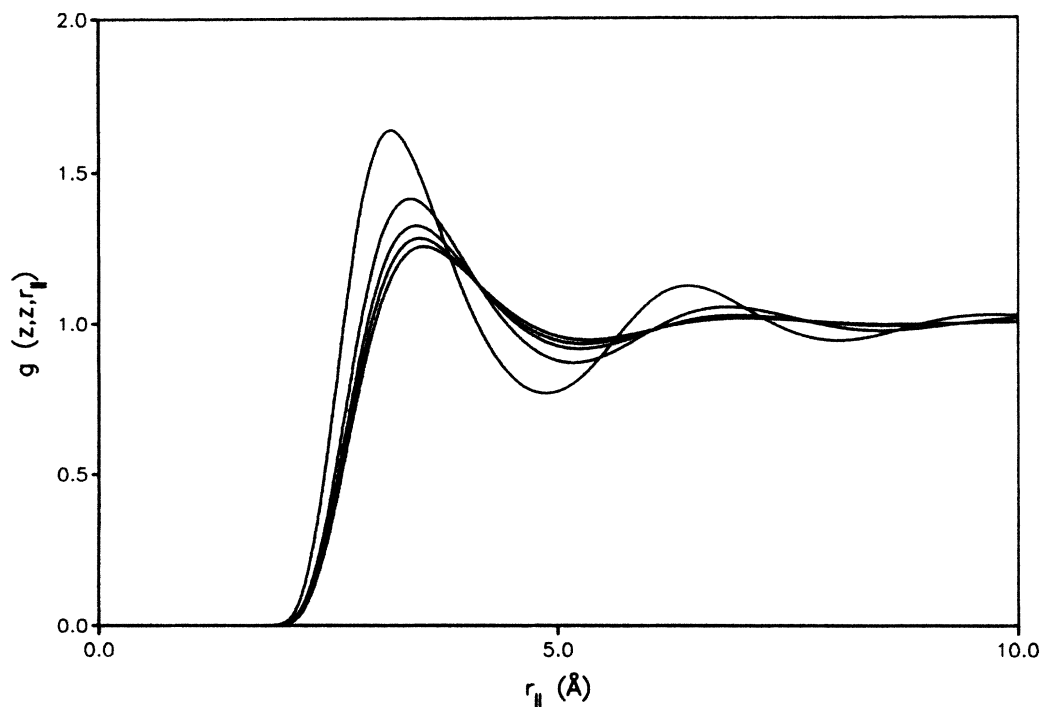


FIG. 6. The pair-distribution function $g(z, z, r_{\parallel})$ is shown for the film with surface coverage of $n = 0.37 \text{ \AA}^{-2}$ in the strong substrate model I, as a function of the distance r_{\parallel} of the two particles parallel to the surface, at the *density maxima*. The function with the strongest nearest-neighbor peak corresponds to the innermost layer at $z = 1.4 \text{ \AA}$ in the coordinate frame of Fig. 1, and the next ones to $z = 4.2, 7.4, 10.6,$ and 13.6 \AA , respectively.

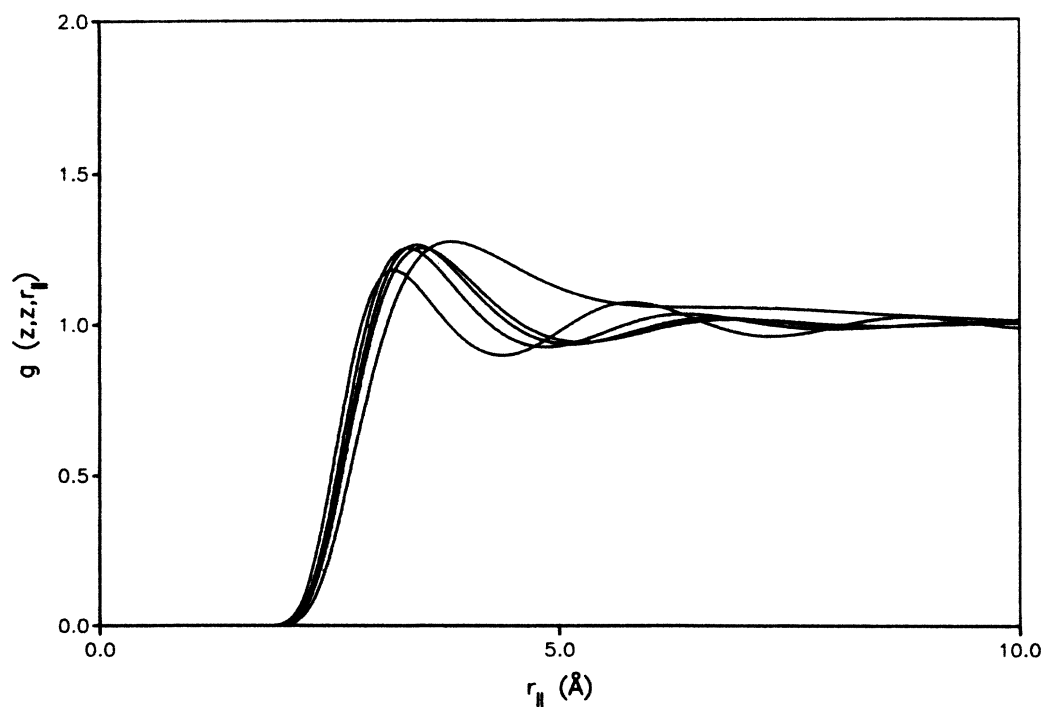


FIG. 7. Same as Fig. 6 for the pair-distribution function at the *density minima*. The function with the smallest nearest-neighbor peak and the shortest-wavelength oscillations corresponds to the innermost density minimum at $z = 2.8 \text{ \AA}$ in the coordinate frame of Fig. 1, and the next ones to $z = 5.8, 9.0,$ and 12.4 \AA , respectively. The structureless function with no oscillations at all corresponds to a point in the surface at $z = 19.0 \text{ \AA}$.

thickness. In the limit of a free surface, $d \rightarrow \infty$, the penetration depth of the surface excitation becomes infinite, and one obtains the familiar ripplon dispersion relation

$$\omega^2 = (\sigma / m\rho) q_{\parallel}^3. \quad (4.2)$$

The form and the dispersion relations of the collective excitations of the helium films are a natural by-product of the optimization of the ground state. The derivation of the connection between the eigenvalues $\hbar\omega_i$ of Eq. (2.21) and the collective excitations¹⁰ assumes a time-dependent component $u_1(\mathbf{r}, t)$ of the Feenberg function (1.1), but *time-independent* two-body correlations. This corresponds to a Feynman wave function for the excited states. The validity of the theory is therefore restricted to wavelengths that are long compared with the interparticle distance, i.e., to the regime of validity of the Feynman-dispersion relation of the bulk liquid.

For fixed wave number q_{\parallel} parallel to the surface, the spectrum has one or more discrete modes²³ with energy $\hbar\omega < -\mu + \hbar^2 q_{\parallel}^2 / 2m$. For energies above $-\mu + \hbar^2 q_{\parallel}^2 / 2m$ the spectrum is continuous.²⁴ The experiment^{5,21} shows a rather rich spectrum of various collective excitations which can, apparently, not all be explained with the Feynman theory. Besides a rather clearly identifiable linear dispersion branch, which we interpret as the surface excitation, one observes very low-lying modes of an almost constant energy and higher-lying collective excitations. Figure 8 compares our results in the momentum regime where the Feynman-dispersion relation is valid, with the experimental results of Refs. 5 and 21. We find that the linear part of the lowest mode comes close to a sequence of experimental points with almost linear dispersion relation. We expect that the remaining

difference is partly due to the inaccuracies of the HNC approximation. Moreover, the zero-sound dispersion relation in the *bulk* is already at a wave number of $q_{\parallel} \approx 1 \text{ \AA}^{-1}$ somewhat below the Feynman-dispersion relation, and we expect a similar effect to appear here due to the assumption of stationary two-body correlations.

A sequence of very low-lying excitations with an energy that is almost independent of the wave number can be observed for $q_{\parallel} > 0.9 \text{ \AA}^{-1}$. These modes apparently cannot be explained within the Feynman theory used here.

A third set of collective modes is observed *above* the surface phonon. These appear in Fig. 8 at the edge of the continuum. Note, however, that the calculated chemical potential is, due to the HNC approximation, about 2 K below the experimental value. Thus, the observed excitations are well below the continuum. It is tempting to identify these excitations with one of the higher-lying discrete modes. An alternative interpretation of these modes is that they are multiple scattering processes from the flat region in the dispersion relation seen at higher momenta.²⁵ Measurements at smaller wavelengths would be helpful to determine the validity of this interpretation.

Figure 9 shows the same dispersion relations for a surface coverage of $n = 0.18 \text{ \AA}^{-2}$, i.e., for a film of about 2.5 layers thickness. The experimental values are included to guide the eye. We see that the lowest mode changes very little, but the distance to the higher-lying excited states increases considerably. In fact, we find only two discrete states in this case. We expect that a better understanding of the nature of the observed higher-lying collective excitations can be gained from measurements for various surface coverages.

Let us finally address the question of the dependence of the excitation spectrum on the substrate potential. Figure 10 shows for a surface coverage of $n = 0.34 \text{ \AA}^{-2}$ a comparison of the dispersion relation of the lowest col-

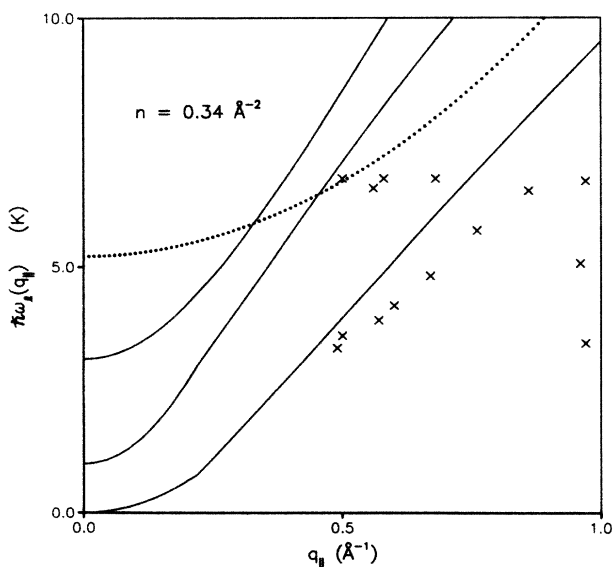


FIG. 8. The dispersion relations of the discrete modes in the helium film with a surface coverage of $n = 0.34 \text{ \AA}^{-2}$ on the hydrogen substrate are compared with the experimental data of Refs. 4 and 18 (crosses) for 6.4 layers of helium on top of a neon-coated graphite powder. The dotted line indicates the lower boundary of the continuum.

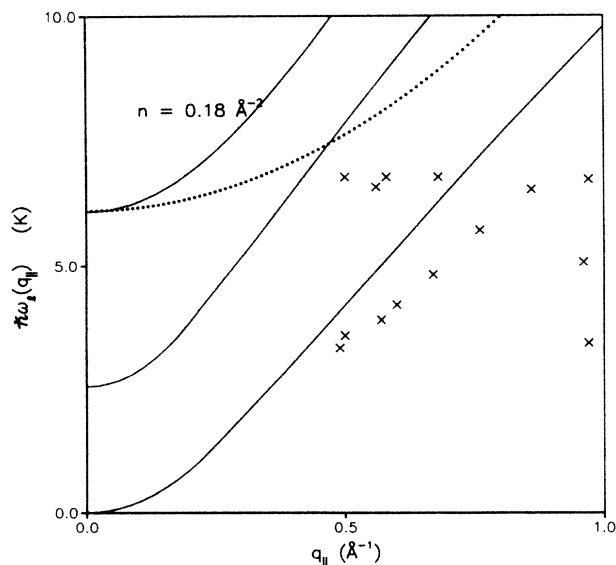


FIG. 9. Same as Fig. 8 for a surface coverage of $n = 0.18 \text{ \AA}^{-2}$.

lective modes for our three substrate potentials. We see a small enhancement of the roton minimum with the strength of the substrate potential. The existence of such a "surface roton" has been speculated;²⁶ we see here that the effect may be present, but is probably too small to be detected experimentally. Our finding is independent of "how close" the system is to a two-dimensional fluid. Figure 11 shows the same dispersion relations for a surface coverage of $n = 0.18 \text{ \AA}^{-2}$, where

$$S(q_{\parallel}, \kappa) = \frac{1}{n} \int d^2 r_{\parallel} \int dz \int dz' e^{-i q_{\parallel} r_{\parallel}} e^{\kappa^* z + \kappa z'} [\rho_1(z)]^{1/2} S(z, z', r_{\parallel}) [\rho_1(z')]^{1/2}. \quad (4.3)$$

To obtain a sufficient intensity in an experimental determination of the static structure function in the surface by neutron scattering requires that the neutrons propagate parallel to the surface. We can therefore restrict our study to the case $\kappa = 0$. Figure 12 shows the static structure function $S(q_{\parallel}, 0)$ for the strong graphite substrate for the two extreme surface coverages $n = 0.12$ and 0.39 \AA^{-2} , and compares them with the bulk static structure function in HNC approximation. We see that all three structure functions are very similar apart from a small enhancement of the peak for the small surface coverages, and a small shift of the peak to larger momenta for the surface structure functions. It remains to be seen whether such differences can be experimentally resolved. We conclude that most of the rich structure of the pair-distribution function shown in Figs. 6 and 7 is averaged out due to the long-wavelength limit $\kappa \rightarrow 0$ taken in Eq. (4.3) in the z direction.

V. LONG-WAVELENGTH LIMIT: THIRD SOUND

Special considerations are required to determine the spectrum of the collective excitations in the long-

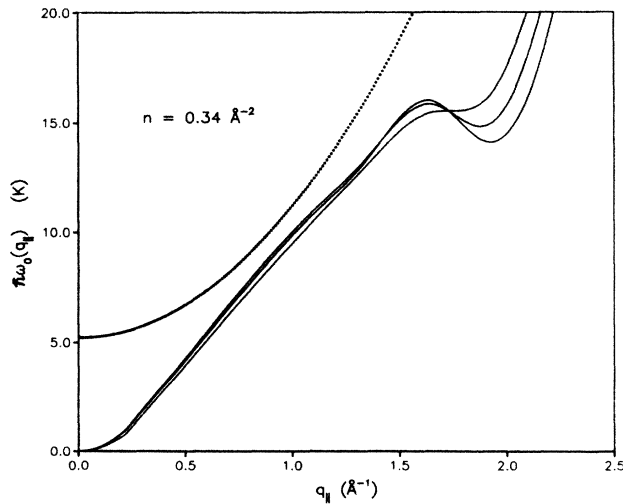


FIG. 10. The dispersion relation of the lowest collective excitation is shown for our three substrate potentials at a surface coverage at $n = 0.34 \text{ \AA}^{-2}$. The curve with the strongest "roton minimum" corresponds to the strongest substrate potential.

the picture is basically unchanged.

The total neutron scattering cross section can be related to the static structure function $S(\mathbf{r}, \mathbf{r}')$ [cf. Eq. (2.26)]. To keep our notation as close as possible to the notation of the bulk theory, we have divided in Eq. (2.26) by two factors of $\sqrt{\rho_1}$. The quantity that is actually measured is the frequency integral of the density fluctuation-correlation function.²⁷ To facilitate comparison with the bulk static form factor, we define

wavelength limit. Note that one cannot extrapolate the dispersion relations derived in the preceding section to $q_{\parallel} \rightarrow 0$ to obtain the long wavelength limit of the dispersion relation: For typical values of the surface tension, the density, and the substrate potential one would conclude that the second term in Eq. (4.1) dominates the first term for wave numbers larger than approximately 0.01 \AA^{-1} . Thus, it is not practical to obtain an estimate for the third-sound velocity from finite-momentum excitation energies. Rather, the long-wavelength limit must be calculated analytically.

We have shown recently²⁸ how the dispersion relation (4.2) can be obtained in linear-response theory from Eq. (2.21). The crucial point in deriving the $q_{\parallel}^{3/2}$ dispersion law was that the operator $H_1 + 2\tilde{V}_{p-h}$ has, in the limit of an infinite half space, a zero eigenvalue as $q_{\parallel} \rightarrow 0$. Note that the operator has to be positive semidefinite in order to have stable collective modes.

In what follows we consider all quantities as functions of z and the wave number q_{\parallel} parallel to the surface. The long-wavelength behavior $\lim_{q_{\parallel} \rightarrow 0} \omega(q_{\parallel})$ of the elementary excitation energy is most easily discussed using variational principles related to the RPA sum rules. For a

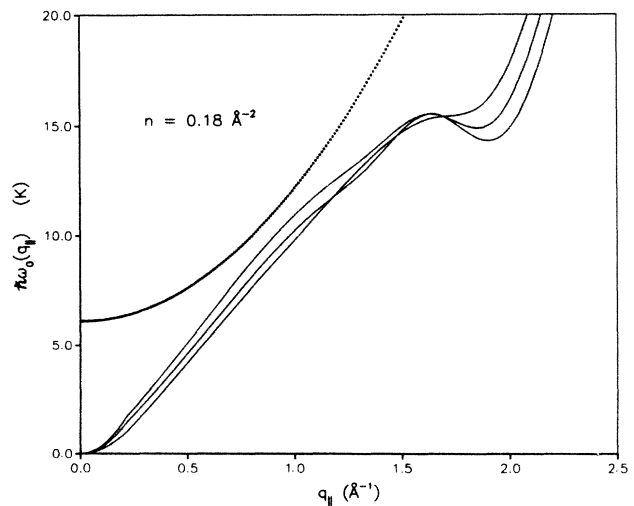


FIG. 11. Same as Fig. 10 for a surface coverage of $n = 0.18 \text{ \AA}^{-2}$.

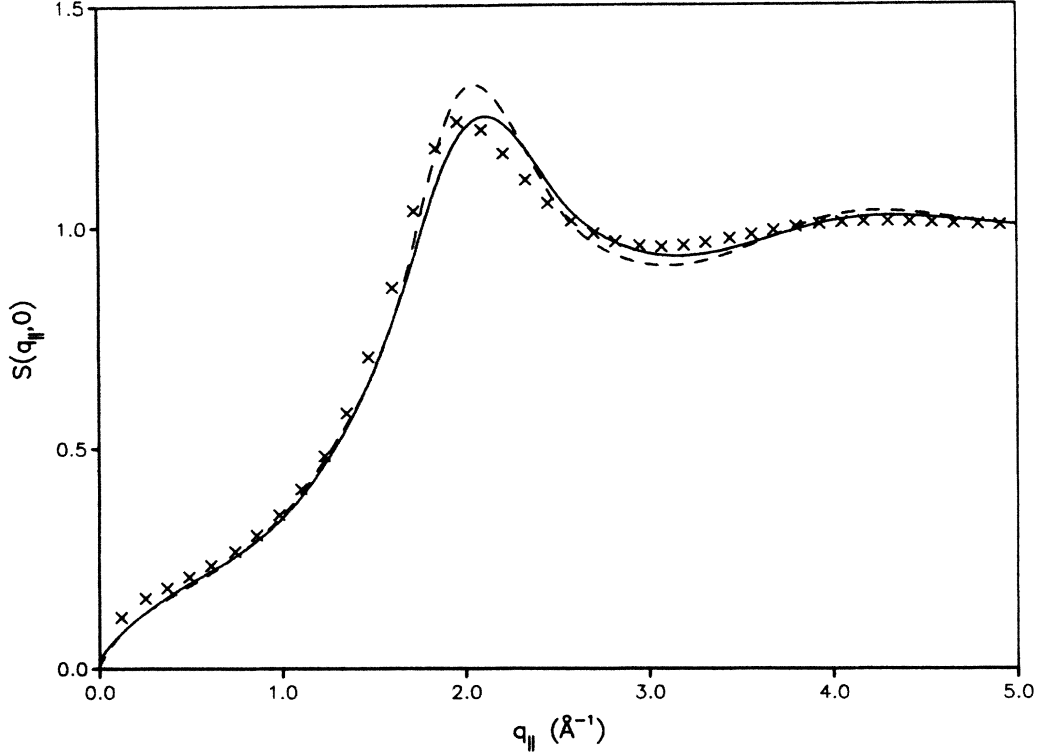


FIG. 12. The static structure factor $S(q_{\parallel}, 0)$ is shown for the strong substrate potential for surface coverages $n = 0.12 \text{ \AA}^{-2}$ (dashed line) and $n = 0.34 \text{ \AA}^{-2}$ (solid line). Also shown is the bulk structure factor in HNC approximation at the calculated equilibrium density (crosses).

given one-body correlation operator

$$F = \sum_i f(\mathbf{r}_i), \quad (5.1)$$

the RPA sum rules are defined as the n th energy-weighted moments of the imaginary part of the RPA response function (2.23) as

$$m_n = \int \frac{d(\hbar\omega)}{2\pi} (\hbar\omega)^n \int d^3r_1 \int d^3r_2 f^*(\mathbf{r}_1) f(\mathbf{r}_2) \times \text{Im}\chi(\mathbf{r}_1, \mathbf{r}_2, \omega). \quad (5.2)$$

From Eqs. (2.21)–(2.23) one obtains the explicit expressions for the sum rules m_3 , m_1 , and m_{-1} :

$$m_3 = (\Psi_f | H_1 (H_1 + 2\tilde{V}_{p-h}) H_1 | \Psi_f), \quad (5.3)$$

$$m_1 = (\Psi_f | H_1 | \Psi_f), \quad (5.4)$$

and

$$m_{-1} = (\Psi_f | (H_1 + 2\tilde{V}_{p-h})^{-1} | \Psi_f), \quad (5.5)$$

where

$$\Psi_f = f(\mathbf{r}) \sqrt{\rho_1(\mathbf{r})}, \quad (5.6)$$

and for convenience we have dropped writing all arguments z , z' , and q_{\parallel} from \tilde{V}_{p-h} . For the long-wavelength limit of \tilde{V}_{p-h} we write

$$\lim_{q_{\parallel} \rightarrow 0} \tilde{V}_{p-h}(q_{\parallel}) = \tilde{V}_{p-h}(0+). \quad (5.7)$$

Note that $\tilde{V}_{p-h}(0+)$ still depends on z and z' .

We see also that minimizing m_3/m_1 or m_1/m_{-1} with respect to the excitation operator,

$$\frac{\delta}{\delta\Psi_f} \frac{m_3}{m_1} = 0 \text{ or } \frac{\delta}{\delta\Psi_f} \frac{m_1}{m_{-1}} = 0, \quad (5.8)$$

is identical to solving the RPA equation (2.21). The quantities m_3/m_1 and m_1/m_{-1} are therefore upper bounds for the square of the exact excitation energy.

From the coordinate/momentum space representation of H_1 in our geometry,

$$\begin{aligned} H_1(q_{\parallel}) &= -\frac{\hbar^2}{2m} \frac{1}{\sqrt{\rho_1(z)}} \frac{d}{dz} \rho_1(z) \frac{d}{dz} \frac{1}{\sqrt{\rho_1(z)}} + \frac{\hbar^2 q_{\parallel}^2}{2m} \\ &= H_1(0) + \frac{\hbar^2 q_{\parallel}^2}{2m}, \end{aligned} \quad (5.9)$$

we conclude that the only way to have a zero excitation energy in the limit $q_{\parallel} \rightarrow 0$ is to have

$$\Psi_f(q_{\parallel}, z) = \sqrt{\rho(z)} + O(q_{\parallel}^2). \quad (5.10)$$

We then obtain

$$\begin{aligned}\hbar^2\omega^2(q_{\parallel}) &= \frac{m_1}{m_{-1}} \\ &= \frac{\hbar^2 q_{\parallel}^2}{2m} \frac{n}{(\sqrt{\rho_1} | [H_1(0) + 2\tilde{V}_{p-h}(0+)]^{-1} | \sqrt{\rho_1})}\end{aligned}\quad (5.11)$$

and we can identify

$$\omega(q_{\parallel}) = c_3 q_{\parallel} \quad (5.12)$$

with

$$mc_3^2 = \frac{1}{2} \frac{n}{(\sqrt{\rho_1} | [H_1(0) + 2\tilde{V}_{p-h}(0+)]^{-1} | \sqrt{\rho_1})}, \quad (5.13)$$

$$\hbar^2\omega^2(q_{\parallel}) \leq \left[\frac{\hbar^2 q_{\parallel}^2}{2mn} \right] (\sqrt{\rho_1} + H_1(0)\delta\Psi | H_1(0) + 2\tilde{V}_{p-h}(0+) | \sqrt{\rho_1} + H_1(0)\delta\Psi). \quad (5.15)$$

Minimization of this expression with respect to $\delta\Psi(z)$ under the constraint of orthogonality gives us again, for $q_{\parallel} \rightarrow 0$, the dispersion relation (5.11) and the shape of the density fluctuation

$$\begin{aligned}\delta\sqrt{\rho_1}(z) &= \lim_{q_{\parallel} \rightarrow 0} H_1(q_{\parallel})\Psi^{(0)}(q_{\parallel}, z) \\ &= \frac{[H_1(0) + 2\tilde{V}_{p-h}(0+)]^{-1} | \sqrt{\rho_1}}{(\sqrt{\rho_1} | [H_1(0) + 2\tilde{V}_{p-h}(0+)]^{-1} | \sqrt{\rho_1})}.\end{aligned}\quad (5.16)$$

The solution (5.16) is normalized such that $(\sqrt{\rho_1} | \delta\sqrt{\rho_1}) = 1$. Of course, the shape of the density fluctuation is also obtained directly in the course of our numerical optimization of the ground state. Typical shapes of the density-fluctuation profile may be found in Ref. 10. A comparison of the shape of the density fluctuation with Eq. (5.12) provides, however, a good test for the numerical accuracy of the calculation.

The calculation of the third-sound velocity c_3 encounters some practical problems. It has already been mentioned that the operator $H_1 + 2\tilde{V}_{p-h}(0+)$ has a zero eigenvalue in the limit of an infinite half space. This is due to the *invariance of the surface profile* under displacements of the surface in the z direction, and hence due to rather subtle cancellations between the attractive and the repulsive parts of the particle-hole interaction. Experimental values^{3,4} for a five-layer film suggest that mc_3^2 should be about 0.8 K. On the other hand, the bulk limit of the particle-hole interaction is mc_1^2 , where c_1 is the value of the *first* sound. The experimental value for this quantity is about 23 K, whereas the calculated value in the HNC approximation is 12 K. In any event, one has to expect cancellations to within more than one order of magnitude. It is therefore no surprise that the calculation of the third-sound velocity becomes numerically very delicate.

These qualifications have to be kept in mind for the interpretation of our numerical results for mc_3^2 . Figure

where c_3 is the third-sound velocity.

The m_1/m_{-1} sum rule is known to be insensitive to inaccurate trial functions; hence we did not need to calculate the correction term of the order q_{\parallel}^2 in Eq. (5.10). This term is needed, however, to obtain the spatial shape of the density fluctuation. To obtain this information, we make the ansatz

$$\Psi_f(q_{\parallel}, z) = \sqrt{\rho_1}(z) + \frac{\hbar^2 q_{\parallel}^2}{2m} \delta\Psi(z), \quad (5.14)$$

and we assume without loss of generality $(\sqrt{\rho_1} | \delta\Psi) = 0$. We then obtain from the m_3/m_1 sum rule,

13 shows the calculated values for mc_3^2 using Eq. (5.13) for the strong graphite substrate potential. To demonstrate the sensitive dependence of this quantity on the particle-hole interaction $V_{p-h}(z, z', q_{\parallel})$ we have performed the calculation for $q_{\parallel} = 0$, $q_{\parallel} = 0.219 \text{ \AA}^{-1}$, and $q_{\parallel} = 0.502 \text{ \AA}^{-1}$. We find that the surface indeed develops a slight instability in the long-wavelength limit in the sense that the right-hand side of Eq. (5.13) becomes negative for thick films. This instability fortunately does not preclude the existence of numerical solutions of the Euler-Lagrange equation, since the $q_{\parallel} = 0$ value is never actually needed. We suspect that this slight instability is a numerical problem. A definite conclusion could be drawn only by repetition of our calculations on a considerably finer mesh, which is presently beyond our computational capabilities. It seems also that such a refinement of the numerics is not yet warranted due to the uncertainties introduced by the HNC approximation and the neglect of three-body correlations, which affect most seriously the sound velocity.

Further evidence that the slight long-wavelength instability is indeed a numerical problem is drawn from the fact that the right-hand side of Eq. (5.13) depends sensitively on the particle-hole interaction. The comparison of the three curves in Fig. 13 shows that the system is already stable if $V_{p-h}(z, z', q_{\parallel})$ is taken for $q_{\parallel} = 0.219 \text{ \AA}^{-1}$ instead of in the limit $q_{\parallel} = 0$, and it reaches its bulk value at $q_{\parallel} = 0.502 \text{ \AA}^{-1}$. It seems obvious from this comparison that the lowest eigenvalue of $H_1 + 2\tilde{V}_{p-h}$ approaches zero quite rapidly as a function of momentum q_{\parallel} , and it is again no surprise that its numerical calculation is quite difficult. We note, however, that a definite statement on the stability of $H_1 + 2\tilde{V}_{p-h}$ in the long-wavelength limit could give microscopic indications for an instability of the surface against very long wavelength (of the order of 50 \text{ \AA}) excitations which might indicate the formation of a corrugated surface. Note, however, that the *chemical potential* is a monotonically increasing function of the surface coverage; in other words our

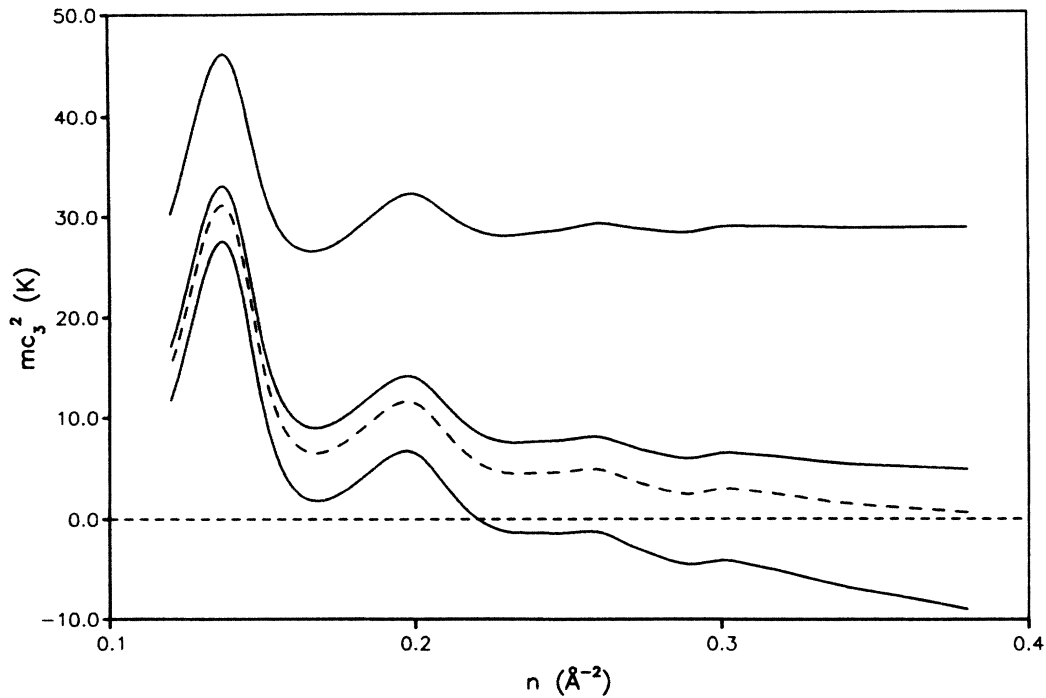


FIG. 13. The estimate for mc_3^2 is shown for the helium films in the strong substrate potential as a function of the surface coverage n . The lowest curve corresponds to the particle-hole interaction $\tilde{V}_{p-h}(z, z', q_{\parallel})$ taken at $q_{\parallel} = 0$, the middle curve to $q_{\parallel} = 0.219 \text{ \AA}^{-1}$, and the upper curve to $q_{\parallel} = 0.502 \text{ \AA}^{-1}$.

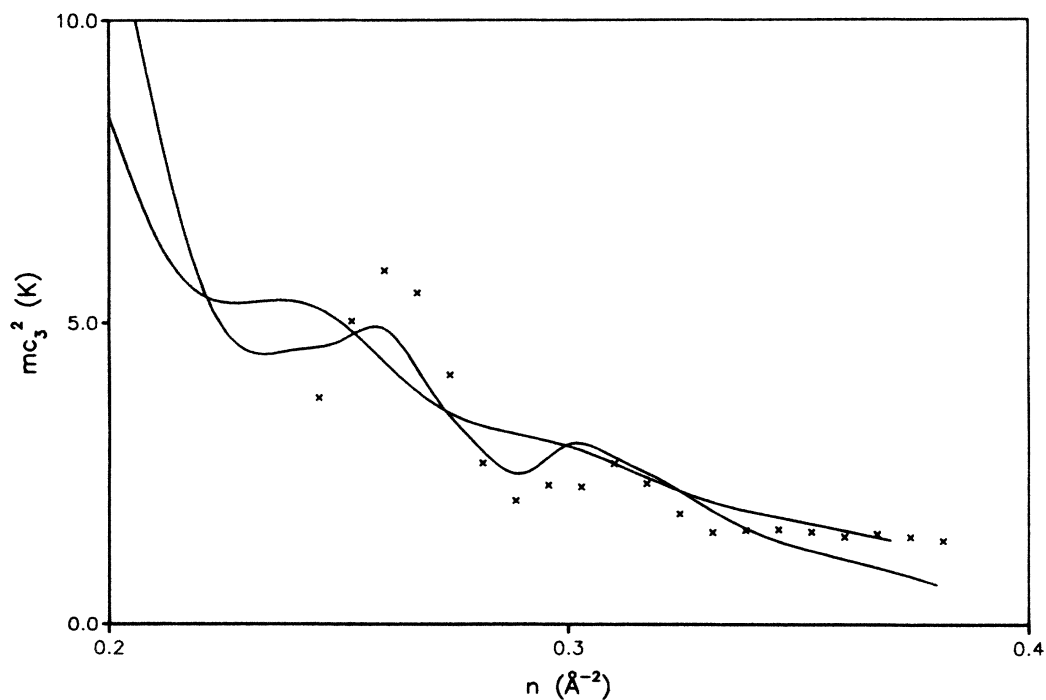


FIG. 14. Our results for mc_3^2 for the medium and the strong substrate potential are compared with the experimental data of Maynard and Chan (Ref. 3, crosses). The experimental data have been modified by a scattering factor of 1.7 and extrapolated to zero temperature as described in the text. The theoretical curves have been obtained by interpolating between the low-momentum portions of the particle-hole interaction. The curve with the strong fluctuations corresponds to the strong substrate potential, and the smoother curve to the medium substrate potential.

theory predicts that all films considered here "wet" the surface. This is in agreement with experimental evidence.⁸

We believe, on the other hand, that the fluctuations of the velocity of sound as a function of the surface coverage are quantitatively significant. We draw this confidence from the fact that their size is essentially the same for the three interactions considered in Fig. 13. To get a reasonable comparison with experimental data,³ we have therefore constructed an estimate for the third-sound velocity by linear interpolation between the calculated particle-hole interaction for $q_{\parallel} = 0$ and 0.219 \AA^{-1} .

The comparison of our interpolated third-sound velocity with the experimental results of Ref. 3 is shown in Fig. 14. The "experimental" results shown there have been obtained from the finite-temperature experiments of Maynard and Chan³ by a linear extrapolation to $T = 0$. More recent data²⁹ on the third-sound resonance frequency reaching to temperatures as low as 0.35 K indicate that such a linear extrapolation is reasonably well justified for surface coverages larger than $n \approx 4.5 \text{ \AA}^{-2}$. The extrapolation somewhat overestimates, presumably, the finite-temperature effects for lower surface coverages. Moreover, a scattering factor³⁰ of 1.7 has been applied to the velocity of sound, and the zero point has been slightly shifted such that the first maximum of the experimental and the theoretical sound velocities coincide. The theoretical predictions and the experimental results coincide in so far as that a *maximum* of the third-sound velocity appears for systems where the last layer is slightly more than half filled, whereas a *minimum* occurs shortly before one layer is completely filled. Our calculations offer some explanation for this. We find (cf. Figs. 1–3) that the $n + 1$ st layer becomes already slightly populated even before the n th layer reaches its maximum density.

Taking all the uncertainties caused on the theoretical side by the HNC approximation and the interpolation procedure for the interactions, and on the experimental side by the extrapolation to zero temperature and the correction for substrate scattering, the agreement between the experimental results and our theoretical description is quite satisfactory. We have mentioned already that the linear extrapolation to zero temperature might somewhat overestimate the true temperature dependence of the third-sound velocity. One would then be led to conclude that our "experimental" third-sound velocity should have somewhat smaller fluctuations.

An interesting feature is the strong dependence of the fluctuations of the third-sound velocity on the substrate potential. The weaker 3-9 potential (model II) shows already much smaller fluctuations, whereas the fluctuations produced by the glass-hydrogen substrate are almost negligible.

VI. SUMMARY

In this paper we have extended the variational description of systems of liquid ⁴He adsorbed to substrates of varying strength, and addressed a number of points of present experimental interest. Despite the well-known quantitative deficiencies of the HNC-EL theory we believe that our description is presently the most powerful one in the sense that a complete theory of the structure and excitations of such systems can be built on minimal assumptions. Similar success of any competing many-body theory remains to be achieved.

Most important from a practical point of view is that our theory gives information on the internal structure of the helium films. The dependence of the chemical potential and the third-sound velocity on the internal structure of the layered liquid comes out of the theory, rather than being input to it, as they would be in hydrodynamic or mean-field models. The quantitative shortcomings of the HNC theory are well understood, and methods to improve upon the accuracy of the microscopic description are available.^{12,13}

Presently it does not seem economical to use a more realistic potential *close* to the substrate. But we feel that the main points studied in this paper and our further plans are not seriously affected by this shortcoming. The lowest-lying collective excitations are localized in the low-density tail of the surface, where only the asymptotic tail of the substrate potential plays a role.

Further improvements and applications of our theory are foreseen in a number of different directions. The interpretation of experiments in which the layer structure of the film is essential naturally provides the most exciting further application. Most predominantly, we mention electron-mobility experiments² and the possibility to generate two-dimensional electron systems in the quantum regime.¹ The theory of electronic states on helium surfaces^{31–35} requires knowledge of the low-lying excitations of the liquid. To the extent that the observations are sensitive to a layer structure,² a theoretical description of the film-thickness dependence of the third-sound velocity seems indispensable, since the experiments of Maynard and Chan³ can apparently not yet resolve such fluctuations up to ten layers.

ACKNOWLEDGMENTS

This work was supported, in part, by the National Science Foundation under Contract No. PHY-85-05979. Stimulating conversations with G. Agnolet, A. J. Dahm, H. Godfrin, H. J. Lauter, P. Leiderer, W. M. Saslow, R. A. Smith, P. Taborek, and H. Wiechert are gratefully acknowledged. We would also like to thank J. D. Maynard for providing Ref. 28 prior to publication.

¹A. J. Dahm and W. F. Vinen, *Phys. Today* **40**(2), 43 (1987).

²M. A. Paalanen and Y. Iye, *Phys. Rev. Lett.* **44**, 333 (1985); D. Cieslikowski, A. J. Dahm, and P. Leiderer, *Phys. Rev. Lett.* **58**, 1751 (1987).

³J. D. Maynard and M. H. W. Chan, *Physica* **109&110B**, 2090 (1982).

⁴J. A. Roth, G. J. Jelatis, and J. D. Maynard, *Phys. Rev. Lett.* **44**, 333 (1980).

⁵H. J. Lauter, H. Godfrin, C. Tiby, H. Wiechert, and P. E. Obermayer, *Surf. Sci.* **125**, 265 (1983).

⁶J. G. Dash and M. Schick, in *Physics of Liquid and Solid Helium*, edited by K. H. Bennemann and J. B. Ketterson (Wiley,

- New York, 1976), Vol. 2.
- ⁷M. Bretz, in *Monolayer and Submonolayer Helium Films*, edited by J. G. Daunt and E. Lerner (Plenum, New York, 1973), p. 11.
- ⁸P. Taborek and L. Senator, *Phys. Rev. Lett.* **57**, 218 (1986).
- ⁹S. Dietrich, in *Phase Transitions and Critical Phenomena*, edited by C. Domb and J. Lebowitz (Academic, London, in press), Vol. 12.
- ¹⁰E. Krotscheck, *Phys. Rev. B* **32**, 5713 (1985).
- ¹¹E. Feenberg, *Theory of Quantum Liquids* (Academic, New York, 1969).
- ¹²C. E. Campbell, *Phys. Lett.* **44A**, 471 (1973); C. C. Chang and C. E. Campbell, *Phys. Rev. B* **15**, 4238 (1977).
- ¹³E. Krotscheck, *Phys. Rev. B* **33**, 3158 (1986).
- ¹⁴R. A. Aziz, V. P. S. Nain, J. C. Carley, W. L. Taylor, and G. T. McConville, *J. Chem. Phys.* **70**, 4330 (1979).
- ¹⁵F. Ricca, *Nuovo Cimento Suppl.* **5**, 339 (1967).
- ¹⁶M. W. Cole, D. R. Frankl, and D. L. Goodstein, *Rev. Mod. Phys.* **53**, 199 (1981).
- ¹⁷W. E. Carlos and M. W. Cole, *Surf. Sci.* **91**, 339 (1980).
- ¹⁸H.-Y. Kim and M. W. Cole, *Phys. Rev. B* **35**, 3990 (1987).
- ¹⁹A. D. Jackson, B. K. Jennings, A. Lande, and R. A. Smith, *Phys. Rev. B* **24**, 105 (1981).
- ²⁰J. DuPont-Roc (private communication).
- ²¹H. J. Lauter, H. Godfrin, and H. Wiechert, in *Proceedings of the Second International Conference on Phonon Physics*, edited by J. Kollár, N. Kroo, M. Meynhard, and T. Siklos (World-Scientific, Singapore, 1985), p. 842.
- ²²H. Wiechert (private communication).
- ²³G. Ji and M. Wortis, *Phys. Rev. B* **34**, 7704 (1986).
- ²⁴Of course, the discretization of the problem on a finite mesh will produce *only* discrete modes (Ref. 10).
- ²⁵W. Götze and M. Lücke, *J. Low Temp. Phys.* **24**, 671 (1976).
- ²⁶W. F. Saam, *Phys. Rev. A* **8**, 1048 (1973).
- ²⁷E. Krotscheck, S. Stringari, and J. Treiner, *Phys. Rev. B* **35**, 4754 (1987).
- ²⁸H. Godfrin (private communication).
- ²⁹S. Kumar, T. Brosius, G. Torzo, D. Finotelle, and J. D. Maynard (unpublished).
- ³⁰J. D. Maynard (private communication).
- ³¹M. W. Cole, *Phys. Rev. B* **2**, 4239 (1970).
- ³²L. M. Sander, *Phys. Rev. B* **11**, 4350 (1975).
- ³³V. B. Shikin and Y. P. Monarkha, *Sov. J. Low Temp. Phys.* **1**, 459 (1975).
- ³⁴S. A. Jackson and P. M. Platzman, *Phys. Rev. B* **24**, 499 (1979).
- ³⁵O. Hippolito, G. A. Farias, and N. Studart, *Surf. Sci.* **113**, 394 (1981).